https://doi.org/10.5194/os-2021-88
Preprint. Discussion started: 22 September 2021
© Author(s) 2021. CC BY 4.0 License.

Ocean Science Discussions

Global distribution and variability of subsurface chlorophyll a concentration

Sayaka Yasunaka[1], Tsuneo Ono[2], Kosei Sasaoka[1], Kanako Sato[1]
[1]Japan Agency for Marine-Earth Science and Technology, Yokosuka, 237-0061, Japan
[2]Japan Fisheries Research and Education Agency, Yokohama, 236-8648, Japan

Correspondence to: Sayaka Yasunaka (yasunaka@jamstec.go.jp)

Abstract. Chlorophyll a (Chl-a) often retains its maximum concentration not at the surface but in the subsurface layer. The depth of the Chl-a maximum primarily depends on the balance between light penetration from the surface and nutrient supply from the deep ocean. However, a global map of subsurface Chl-a concentrations based on observations has not been presented yet. In this study, we integrate Chl-*a* concentration data not only from recent biogeochemical floats but also from historical ship-based and other observations, and present global maps of subsurface Chl-*a* concentration with related variables. The subsurface Chl-*a* maximum deeper than the mixed layer depth was stably observed in the subtropics and tropics (30°S to 30°N), only in summer in midlatitudes (30–40°N/S), and rarely at 45–60°S of the Southern Ocean and in the northern North Atlantic (north of 45°N). The depths of the subsurface Chl-*a* maxima are deeper than those of the euphotic layer in the subtropics and shallower in the tropics and midlatitudes. In the subtropics, seasonal oxygen increases below the mixed layer implied substantial biological new production, which corresponds to 10% of the net primary production there. During El Niño, the subsurface Chl-*a* concentration in the equatorial Pacific is higher in the middle to the east and lower in the west than that during La Niña, which is opposite that on the surface. The spatiotemporal variability of the Chl-a concentration described here would be suggestive results not only for the biogeochemical cycle in the ocean but also for the thermal structure and the dynamics of the ocean via the absorption of shortwave radiation.

1 Introduction

Chlorophyll *a* (Chl-*a*) concentration in the ocean often retains its maximum value not at the surface but in the subsurface layer. The subsurface Chl-*a* maximum is a widespread and common feature in various oceans in the tropics, subtropics, and subarctic (Anderson, 1969; Saijo et al., 1969; Furuya, 1990; Bhattathiri et al., 1996; Mann and Lazier, 1996). It is also recently reported in the Arctic Ocean and the Southern Ocean (Ardyna et al., 2013; Baldry et al., 2020). Substantial primary production is also observed in the subsurface, although the relationship among Chl-*a* concentration, biological biomass, and primary production is not simple (Campbell and Vaulot, 1993; Goldman, 1988; Fennel and Boss, 2003; Matsumoto and Furuya, 2011; Cornec et al., 2021). The depth of the Chl-*a* maximum primarily depends on the balance between light penetration from the surface and nutrient supply from the deep ocean (Cullen, 2015) and partly on light-dependent grazing by zooplankton near the surface (Moeller et al., 2019).

https://doi.org/10.5194/os-2021-88
Preprint. Discussion started: 22 September 2021
© Author(s) 2021. CC BY 4.0 License.


Chl-*a* concentration affects the ocean physically. Chl-*a* absorbs shortwave radiation, which leads to ocean warming and then modifies the thermal structure and the dynamics of the ocean (Lewis et al., 1990; Siegel et al., 1995). Modeling studies indicated that Chl-*a* concentration plays a precursor of the El Niño event (Park et al. 2018) and interannual variation of subsurface Chl-*a* concentration is an important parameter on the El Niño simulation (Jochum et al., 2010; Kang et al. 2018).

Using satellite-retrieved ocean surface Chl-*a* concentrations, many studies have described the basin-wide spatial distribution and temporal variation of surface Chl-*a* (Dunstan et al., 2018; Lin et al., 2014; Sasaoka et al., 2011). However, those of subsurface Chl-*a* had not been clarified. Although several studies parameterized the vertical profile of Chl-*a* concentrations and reproduced subsurface Chl-*a* maxima (Ardyna et al., 2013; Uitz et al., 2006), their main purpose was estimating depth-integrated Chl-*a* and primary production. Recently, Biogeochemical Argo floats with Chl-*a* sensors have revealed occurrence of the subsurface Chl-*a* maxima and their relationship with a phytoplankton biomass in the world ocean (Cornec et al., 2021). However, because coverage of subsurface Chl-a data derived from a single data source is not enough to illustrate it, a global map of subsurface Chl-a concentrations based on observations has not been presented yet. Global maps of subsurface Chl-a maximum have so far been based on statistical estimates or numerical models (Mignot et al., 2014; Masuda et al., 2021). Therefore, only surface Chl-a concentration is used as validation data for numerical models (e.g. Séférian et al. 2020).

Here, we synthesize Chl-*a* concentration data not only from recent biogeochemical floats but also from historical ship-based and other observations, and present global maps of subsurface Chl-*a* concentration. Then, we clarify seasonal and interannual variability of subsurface Chl-*a* concentration with other related variables in the world ocean.

2 Data

Chl-*a* measurements were extracted from the World Ocean Database 2018 (WOD2018; Boyer et al., 2018; https://www.nodc.noaa.gov/OC5/WOD/pr_wod.html) and the Global Ocean Data Analysis Project version 2.2019 Release (GLODAPv2.2019; Olsen et al., 2019; https://www.glodap.info/). These measurements were from bottle samples, CTD fluorescence, towed CTD fluorescence, profiling floats, gliders, and drifting buoys. Data from Biogeochemical Argo floats are included in WOD2018 as data from profiling floats. The number of Chl-*a* data measurements totaled 114,107,161 from 737,469 profiles from 1932 to 2020 in the upper 300 m. Most of the data in the open ocean are from bottle samples, CTD fluorescence and profiling floats (Figure S1).

We calculated the depth of the Chl-*a* maximum in each profile, which includes data from more than five different depths and then binned them into 1° × 1° × 1-month grid cells (regardless of the year). The sampling depth interval of the Chl-*a* maximum is 7 m on average (3 m in CTD fluorescence and profiling floats, and 16 m in bottle samples). The depths of the Chl-*a* maximum are generally similar among different data sources: deeper than 80 m in the subtropics and 40 m in the tropics and the Southern Ocean (Figure S1 in the Supporting Information). The Chl-*a* concentrations at the maximum are also similar among different data sources: greater than 0.5 mg/m^3 north of 30°N, south of 50°S, the northern Indian Ocean, and coastal areas; less than 0.2 mg/m^3 in the central subtropics; and 0.2–0.5 mg/m^3 in other regions, although extraordinary

https://doi.org/10.5194/os-2021-88
Preprint. Discussion started: 22 September 2021
© Author(s) 2021. CC BY 4.0 License.


low or high concentrations along some specific lines and areas can be seen (Figure S2). Therefore, we treated data together from all data sources.

We also calculated monthly means of Chl-*a* concentration in 1° × 1° grid cells at the depths of 5 m (0–5 m), 10 m (5–15 m), 20 m (15–25 m), 30 m (25–40 m), 50 m (40–62.5 m), 75 m (62.5–87.5 m), 100 m (87.5–112.5 m), 125 m (112.5–137.5 m), 150 m (137.5–175 m), and 200 m (175–250 m). We conducted the following quality control measures to reduce the effect of erroneous data or data in short-term and small-scale extreme conditions:

1. We calculated the long-term mean and its standard deviation within ±5° latitude, ±10° longitude, and ±1 month (regardless of the year) for each 1° × 1° × 1-month grid cell at each depth.
2. We eliminated data that differed by more than three standard deviations from the long-term mean in each grid cell at each depth.
3. We eliminated profiles in which more than half of all data had been eliminated in Step 2.
4. We eliminated profiles in which more than half of all profiles within ±10° of the latitude and longitude had been eliminated in Step 3.

This procedure identified approximately 2% of the measurements as erroneous or extreme values.

Satellite-derived surface Chl-*a* concentrations, euphotic layer depths, and photosynthetically available radiation (PAR) with 1° × 1° monthly resolutions since September 1997 were downloaded from the website of the GlobColour project (GlobColour_R2018; http://hermes.acri.fr/index.php; Frouin et al., 2003; Maritorena et al., 2010; Moor et al., 2007). Monthly fields of net primary production (NPP) were obtained from the Ocean Productivity website (http://www.science.oregonstate.edu/ocean.productivity/index.php) with a spatial resolution of 1/6° × 1/6°, which were calculated using the vertically generalized production model of Behrenfeld and Falkowski (1997). We used climatological means of oxygen concentrations, oxygen saturation ratios, and nitrate concentrations in the World Ocean Atlas 2018 (WOA2018; https://www.nodc.noaa.gov/OC5/woa18/; Garcia et al., 2018a, 2018b). We also used climatological means of mixed layer depths (the depth with a change from the surface sigma-θ of 0.125) produced by JAMSTEC (MILA_GPV; http://www.jamstec.go.jp/ARGO/argo_web/argo/?page_id=223andlang=en; Hosoda et al. 2010; missing data were interpolated using data in the surrounding grids).

We calculated the Niño 3.4 index (sea surface temperature over 5°N to 5°S, 170–120°W) for an index of El Niño and La Niña by using the Hadley Centre Sea Ice and Sea Surface Temperature data set (HadISST; https://www.metoffice.g.,ov.uk/hadobs/hadisst/; Rayner et al., 2003). El Niño or La Niña events were originally defined by the Niño 3.4 index exceeding ±0.4°C for 6 months or longer (Trenberth, 1997). Here, El Niño or La Niña events represent all positive or negative Niño 3.4 indices respectively because the amount of subsurface Chl-a data would otherwise be limited.

https://doi.org/10.5194/os-2021-88
Preprint. Discussion started: 22 September 2021
© Author(s) 2021. CC BY 4.0 License.

Ocean Science Discussions

3 Result

3.1 Climatological mean state

The depths of the Chl-*a* maxima from all profiles and cross-sections of Chl-*a* concentration from the quality-controlled data are shown in Figures 1a and 2, respectively. We selected the central latitudinal and longitudinal bands of the subtropics, the tropics, the Indian Ocean, the Pacific Ocean, and the Atlantic Ocean in Figure 2. The Chl-*a* concentration shows the subsurface maxima in large parts of the subtropics and tropics at depths below 80 and 40 m, respectively. The depth of the subsurface maximum is deeper than 120 m in the central subtropics and reaches 150 m approximately 25°S, 100°W in the South Pacific. The subsurface maxima in the subtropics and the tropics were deeper than the mixed layer (Figures 3a and 4). In the Southern Ocean and the northern North Atlantic, several patches of subsurface maxima at depths greater than 80 m can be seen, however, these depths are generally shallower than the mixed layer depth (Figures 1a, 3a, and 4d–f). The Chl-*a* concentrations at the subsurface maxima are 0.1–0.2 mg/m^3 in the subtropics, 0.2–0.5 mg/m^3 in the tropics, and >0.5 mg/m^3 in the subarctic (Figures 1e and 2).

The long-term mean of the euphotic layer depth is greater than 80 m in the subtropics, south of 60°S, and the Arctic Ocean and deeper than 40 m in other regions (Figure 1b). The euphotic layer depth is greater than the mixed layer depth in the subtropics, south of 60°S, the Arctic Ocean, and the tropics but shallower in the northern subtropics and the Southern Ocean (Figures 1b and 4). The spatial distribution of the euphotic layer depth is similar to that of the subsurface Chl-*a* maximum depth (Figure 1a and b), but a substantial difference can be found (Figures 3 and 4). The depth of the subsurface Chl-*a* maximum is greater than the euphotic layer depth in the subtropics but shallower than the euphotic layer depth in other regions.

The nitrate concentration is less than 1 μmol/kg in the surface layer where the subsurface Chl-*a* maximum is deep (Figures 1c and 4). The nitrate concentration at the deep subsurface Chl-*a* maximum is also low (Figure 1f). At the subsurface Chl-*a* maximum, the nitrate concentration is greater than 5 μmol/kg in the subarctic and eastern tropics but less than 1 μmol/kg in the subtropics and the Arctic Ocean.

The subtropics are mostly oversaturated with oxygen mainly at depths greater than 40 m and at 80 m or deeper in some places (Figures 1d and 4). The lower limit of oxygen oversaturation in the subtropics is mostly below the mixed layer and above the subsurface Chl-*a* maximum (Figures 1d and 3c).

3.2 Seasonal variation

The subsurface Chl-*a* maximum in the subtropics can be seen during both winter and summer (Figures 5a and 6) below the mixed layer in both seasons (Figure 6). The euphotic layer is deeper than the mixed layer between 20°N and 30°S in the Indian Ocean and the western Pacific and between 20°N and 20°S in the Atlantic Ocean and the eastern Pacific in both seasons, and in the whole summer hemisphere (Figures 5b, 6d, and 6e). The summer deepening of the euphotic layer is more than 15 m in the 20° to 40° latitudinal bands in both hemispheres (Figures 5e and 6f). North of 50°N and south of 60°S, the

https://doi.org/10.5194/os-2021-88
Preprint. Discussion started: 22 September 2021
© Author(s) 2021. CC BY 4.0 License.


euphotic layer is deeper in winter than in summer. The seasonal difference in the Chl-*a* maximum depth shows the same tendency as that of the euphotic layer (Figure 5d). Oxygen below the mixed layer is oversaturated north of 10°N and in 10–45°S in summer (Figures 5c, 6b, 6d, and 6e). The subsurface oxygen concentration is higher in summer than in winter at approximately 15° to 40° latitudes (Figures 5f, 6c, and 6f).

Counting the months when the Chl-*a* maximum was deeper than the mixed layer, the subsurface Chl-*a* maximum was observed stably in the subtropics and tropics (30°S to 30°N), only in summer in midlatitudes (30° to 40°), and rarely at 45–60°S of the Southern Ocean and in the northern North Atlantic (north of 45°N) (Figures 7a and 8). Here, the Chl-*a* maxima shallower than the mixed layer were not taken into account because they are often contaminated with the subsurface fluorescence maximum (see Section 4). Ratio of months when the euphotic layer was deeper than the mixed layer shows similar pattern to ratio when the euphotic layer was deeper than the subsurface Chl-*a* maximum except for the northern North Atlantic (Figure 7b). In the midlatitudes, the Chl-*a* concentrations were high in the whole mixed layer in winter and still high in the subsurface but low on the surface in summer when the mixed layer becomes shallow (Figure 8c). At 45–60°S of the Southern Ocean and the northern North Atlantic, the Chl-*a* concentration was high in the mixed layer in summer and low in winter (Figure 8h and 8i). In the subarctic North Pacific, the seasonal cycle of the Chl-*a* concentration is similar to that in the subarctic North Atlantic, although the surface Chl-*a* concentration is relatively low and the subsurface Chl-*a* maximum appears under the mixed layer in midsummer (Figure 8g).

3.3 El Niño–Southern Oscillation (ENSO)-related variation

A subsurface Chl-*a* maximum along the equator can be seen during El Niño and La Niña (Figure 9a and 9b). Below the mixed layer, the Chl-*a* concentration is lower west of 160°E during El Niño but higher east of 170°W (Figure 9c). Although the difference in the Chl-*a* concentrations between El Niño and La Niña is noisy above the mixed layer, most of the significant difference is negative east of 150°E (Figure 9c). Satellite-derived surface Chl-*a* concentrations show lower values during El Niño than those during La Niña east of 150°E in line with the Chl-*a* change from the profile data (Figure 9d). The euphotic layer is deeper, and PAR is weaker during El Niño east of 150°E (Figure 9e and 9f).

4 Discussion

The spatial distribution of the subsurface Chl-*a* maximum in the subtropics shown in the present study (Figures 1a and 2) corresponds to the bowl-shaped thermocline structure of the subtropical gyre (Pedlosky, 1990). The deep thermocline in the central subtropics suppresses nutrient supply to the surface, causing low nutrient and Chl-*a* concentrations therein.

Uitz et al. (2006) explained that the greater depth of the subsurface Chl-*a* maximum corresponds to lower surface Chl-*a* concentrations because light proceeds until it is absorbed by chlorophyll. Our study showed that the depth of the subsurface Chl-*a* maximum is roughly consistent with the depth of the euphotic layer in the world ocean (Figure 1a and 1b). However, Chl-*a* in the central subtropics retains maximum concentrations at weaker than 1% light levels, the so-called twilight zone (Figures 3 and 4). This is because nutrient concentration is quite low in the surface layer and light scatters away until it

https://doi.org/10.5194/os-2021-88
Preprint. Discussion started: 22 September 2021
© Author(s) 2021. CC BY 4.0 License.


reaches a layer where nutrients are available (Beckmann and Hense, 2007). Also, PAR at the bottom of the euphotic layer is relatively large in the subtropics (Letelier et al. 2004), and photoacclimation allow Chl-*a* to increase in the low PAR layer (Cornec et al. 2021; Masuda et al. 2021). When nutrients are available at a shallow layer, Chl-*a* retains maximum concentrations at stronger than 1% light level as in the tropics and subarctic (Figures 1, 3, and 4). Note that Chl-*a* concentrations below the Chl-*a* maximum are still significant, including those below the euphotic layer in the tropics and subarctic (Figure 2).

The subsurface Chl-*a* maxima deeper than the mixed layer, in the world ocean can be categorized into three types depending on their seasonal cycles: (a) stable maximum all year round in the subtropics and tropics (30°S to 30°N); (b) summer maximum in the midlatitudes (30° to 40°); and (c) rare maximum in 45–60°S of the Southern Ocean and the northern North Atlantic (north of 45°N) (Figures 7 and 8). The category of the subsurface Chl-*a* maximum also corresponds with the seasonal cycle of the surface Chl-*a*. Surface Chl-*a* is subjected to nutrient limitation and is low in all seasons in region A (Figure 8a, 8b, and 8d–f). In region B, nutrients are supplied by winter mixing, and a surface bloom is observed in winter; in contrast, surface nutrients get depleted, and the main body of Chl-*a* is left in the subsurface in summer (Figure 8c). In region C, the surface Chl-*a* concentrations increased after the shallowing of the mixed layer and with sufficient light in summer (Figure 8h and 8i). These features are consistent with regional studies in the literature (e.g., Baldry et al., 2020; Fujiki et al., 2020; Mignot et al. 2014; Sverdrup, 1953). The latitudinal dependence of the occurrence of the subsurface Chl-*a* maxima also pointed out in Cornec et al. (2021). The low surface Chl-*a* concentration and subsurface Chl-*a* maximum under the mixed layer in midsummer in the subarctic North Pacific (Figure 8g) are due to iron limitations at the surface (Martin and Fitzwater, 1988; Nishioka and Obata, 2017). The Chl-*a* concentration in the subarctic shows a vertical gradient within the deep mixed layer in winter (Figures 6d, 6e and 8g–8i) probably because it increases with sporadic stratification (Ito et al., 2015).

Because the patches of the subsurface maxima deeper than 80 m in the Southern Ocean and the northern North Atlantic were mainly derived from profiling floats and often shallower than the mixed layer depth (Figures S1d and 3a), they would not be the subsurface Chl-*a* maximum but the subsurface fluorescence maximum (Falkowski and Kolber, 1995; Biermann et al., 2015). Meanwhile, south of 60°S in the eastern Indian sector of the Southern Ocean, the subsurface Chl-*a* maximum is deeper than the mixed layer (Figure 3a). Actually, a subsurface Chl-*a* maximum after a sea ice retreat has been reported there (Gomi et al., 2007).

In the subtropics, nitrate concentrations were quite low even at the depths of the Chl-*a* maximum (Figure 1f). Nitrate concentration is not necessarily the index of available nutrients for phytoplankton. Nitrate is used as soon as it is supplied in the subtropics (Lewis et al., 1986). Biological production does not always require nitrate, and ammonium assimilation is more important in the subtropics than in the subarctic (Eppley and Peterson, 1979). Nitrogen fixation also contributes to biological production in the subtropics (Deutsch et al., 2007; Karl et al., 1997). Meanwhile, nitrate concentrations are high at the depths of the Chl-*a* maximum in the subarctic North Pacific and in the eastern tropical Pacific because the limiting factor of biological production is not nitrate but iron (Landry et al., 1997; Martin and Fitzwater, 1988; Martin et al., 1990).

https://doi.org/10.5194/os-2021-88
Preprint. Discussion started: 22 September 2021
© Author(s) 2021. CC BY 4.0 License.


Oxygen oversaturation in the subtropics can be seen below the mixed layer depth and above the subsurface Chl-*a* maximum (Figures 1d, 3c, and 4). Biological production per Chl-*a* concentration is generally more effective under high light levels (Yoder, 1979). The generated oxygen in the deeper layer would be cancelled out by the remineralisation of sinking particles (Martin et al., 1987). In any case, substantial new production is in the subtropics. Seasonal oxygen production in the subtropical subsurface layer from winter to summer sometimes retains approximately 5–10 μmol/kg of oxygen (Figures 5f, 6c, and 6f). When the seasonal oxygen production is integrated into the 50–150-m depth, it becomes 500–1000 mmolO/m^2/6 months. Assuming a Redfield ratio of 276O:106C, it is converted to 200–400 mmolC/m^2/6 months. This is consistent with the net community production values of 1.6 ± 0.2 molC/m^2/yr and 0.9 ± 0.4 molC/m^2/yr, half of which were in the surface layer, in the subtropical North and South Pacific by Riser and Johnson (2008). The satellite-derived NPP in the subtropics is approximately 20 mmol/m^2/day and 3600 mmolC/m^2/6 months (not shown here). Consequently, new production derived from subsurface oxygen production in the subtropics is estimated at approximately 10% of the NPP. This is consistent with the f-ratio of 15% reported at station ALOHA (23°N 158°W; Karl et al., 1996), considering small but nonzero seasonal dissolved inorganic carbon drawdown reported in the subtropical surface layer (Yasunaka et al., 2013, 2021). However, it should be noted that oxygen production is sometimes not associated with biomass increase in shallow layers in the subtropics (Fujiki et al., 2020).

Seasonal nitrate reduction with oxygen production in subsurface layers cannot be deduced (not shown here), probably because the number and quality of nitrate observations are insufficient for detection. Another possibility is that nitrogen fixation substantially contributes to biological production (Deutsch et al. 2007; Karl et al., 1997).

Lower Chl-*a* concentrations at the surface during El Niño (Figure 9c and 9d) result from the reduced upwelling of nutrient-rich subsurface water to the surface (Chavez et al., 1999). Although Matsumoto and Furuya (2011) showed that subsurface Chl-*a* concentrations averaged in the western Pacific warm pool region had no substantial change associated with ENSO, subsurface Chl-*a* concentrations at the fixed grids decrease during El Niño west of 160°E (Figure 9c).

The inverse correlation of the surface and subsurface Chl-*a* concentrations in the central and eastern tropical Pacific associated with ENSO (Figure 9c) may be because a decrease in surface Chl-*a* concentrations increases light intrusion to the subsurface (Figure 9d and 9e). This then increases the subsurface Chl-*a* concentrations, as Uitz et al. (2006) formulated. In Uitz et al. (2006), the Chl-*a* profile in stratified water is parameterized to increase the subsurface Chl-*a* concentrations with decreasing surface Chl-*a* concentrations. The inverse correlation associated with ENSO has been presented in model results (Lee et al., 2014; Kang et al., 2019). However, the subsurface signals in those models are much weaker than the surface signals, unlike those in this study (see Figure 4 in Uitz et al., 2006, and Figure 11 in Lee et al., 2014). Thus, the subsurface response in this process may have been underestimated.

5 Conclusion

The present study provides the first view of the global maps of subsurface Chl-*a* maxima and their seasonal variation and interannual variation associated with ENSO. Using in situ Chl-*a* concentration data, we found the dynamic variability of

https://doi.org/10.5194/os-2021-88
Preprint. Discussion started: 22 September 2021
© Author(s) 2021. CC BY 4.0 License.


subsurface Chl-*a* concentration in time and space. The subsurface Chl-*a* maximum was observed stably in the subtropics and tropics (30°S to 30°N), only in summer in the midlatitudes (30–40°N/S), and rarely at 45–60°S of the Southern Ocean and in the northern North Atlantic (north of 45°N). It extends deeper than the bottom of the euphotic layer in the subtropics but shallower in the tropics and midlatitudes. The subsurface Chl-*a* maxima at 20° to 40° latitudinal bands tend to deepen in summer with the seasonal deepening of the euphotic layer. The seasonal oxygen increase below the mixed layer in the subtropics implied substantial biological new production. During El Niño, the subsurface Chl-*a* concentrations in the equatorial Pacific are higher in the middle to the east and lower in the west than that during La Niña, which is opposite that on the surface.

Chl-*a* concentration varies dynamically in time and space not only on the surface but also in the subsurface ocean. The maps presented in this study would be useful to validate ocean biogeochemical and Earth system models and should facilitate development of the models. Chl-*a* concentration also relates to the absorption of shortwave radiation, and the vertical distribution of shortwave radiation affects the thermal structure and the dynamics of the ocean (Lewis et al., 1990; Siegel et al., 1995). Therefore, continuously measuring and archiving Chl-*a* data are desirable. Increasing the coverage of biogeochemical floats with Chl-*a* sensors is a promising way of increasing subsurface Chl-*a* data (Chai et al., 2020).

Data availability

All data used in the present paper are available in the website referred to in the text.

Author contribution

SY designed the study, conducted the analysis, and wrote the manuscript. TO conceived the study and modified the manuscript. KS provided advice on the analysis and the manuscript. KS helped with data management.

Competing interests

The authors declare that they have no conflict of interest.

Acknowledgment

This work was financially supported by JSPS KAKENHI (Grant Number JP18H04129).

https://doi.org/10.5194/os-2021-88
Preprint. Discussion started: 22 September 2021
© Author(s) 2021. CC BY 4.0 License.


References

Anderson, O. R.: An interdisciplinary theory of behavior. Journal of Research in Science Teaching, 6, 265–273, doi:10.1002/tea.3660060311, 1969.

Ardyna, M., Babin, M., Gosselin, M., Devred, E., Bélanger, S., Matsuoka, A., and Tremblay, J. -É.: Parameterization of vertical chlorophyll a in the Arctic Ocean: Impact of the subsurface chlorophyll maximum on regional, seasonal, and annual primary production estimates, Biogeosciences, 10, 4383–4404, doi:10.5194/bg-10-4383-2013, 2013.

Baldry K., Strutton, P. G., Hill, N. A., and Boyd, P. W.: Subsurface chlorophyll-a maxima in the Southern Ocean, Frontiers in Marine Science, 7, 671, doi:10.3389/fmars.2020.00671, 2020.

Beckmann, A. and Hense, I.: Beneath the surface: Characteristics of oceanic ecosystems under weak mixing conditions—a theoretical investigation, Progress in Oceanography, 75, 771–796, doi:10.1016/j.pocean.2007.09.002, 2007.

Behrenfeld, M. J. and Falkowski, P. G.: Photosynthetic rates derived from satellite-based chlorophyll concentration, Limnology and Oceanography, 42, 1–20, doi:10.4319/lo.1997.42.1.0001, 1997.

Bhattathiri, P. M. A., Pant, A., Sawant, S. S., Gauns, M., Matondkar, S. G. P., and Mohanraju, R.: Phytoplankton production and chlorophyll distribution in the eastern and central Arabian Sea in 1994-1995, Current Science, 71, 857–862, http://drs.nio.org/drs/handle/2264/2149, 1996

Biermann, L., Guinet, C., Bester, M., Brierley, A., and Boehme, L.: An alternative method for correcting fluorescence quenching, Ocean Science, 11, 83–91, doi:10.5194/os-11-83-2015, 2015.

Boyer, T. P., Baranova, O. K., Coleman, C., Garcia, H. E., Grodsky, A., Locarnini, R. A., Mishonov, A. V., Paver, C. R., Reagan, J. R., Seidov, D., Smolyar, I. V., Weathers, K., and Zweng, M. M.: World Ocean Database 2018, A.V. Mishonov, Technical Ed.; NOAA Atlas NESDIS 87, 2018.

Campbell, L. and Vaulot, D.: Photosynthetic picoplankton community structure in the subtropical North Pacific Ocean near Hawaii (station ALOHA), Deep Sea Research Part I, 40, 2043–2060, doi:10.1016/0967-0637(93)90044-4, 1993.

Chai, F., Johnson, K.S., Claustre, H., Xing, X., Wang, Y., Boss, E., Riser, S., Fennel, K., Schofield, O., and Sutton, A.: Monitoring ocean biogeochemistry with autonomous platforms, Nature Reviews Earth and Environment, 1, 315–326. doi:10.1038/s43017-020-0053-y, 2020.

Chavez, F. P., Strutton, P. G., Friederich, G. E., Feely, R. A., Feldman, G. C., Foley, D. G., and McPhaden, M.J.: Biological and chemical response of the equatorial Pacific Ocean to the 1997-98 El Niño, Science, 286, 2126–2131. doi:10.1126/science.286.5447.2126, 1999.

Cornec, M, Claustre, H., Mignot, A., Guidi, L., Lacour, L., Poteau, A., D'Ortenzio, F., Gentili, B., and Schmechtig, C.: Deep Chlorophyll Maxima in the Global Ocean: Occurrences, Drivers and Characteristics, Global Biogeochemical Cycles, 35, e2020GB006759, doi:10.1029/2020GB006759, 2021.

Cullen, J. J.: Subsurface chlorophyll maximum layers: Enduring enigma or mystery solved? Annual Review of Marine Science, 7, 207–239, doi:10.1146/annurev-marine-010213-135111, 2015.

https://doi.org/10.5194/os-2021-88
Preprint. Discussion started: 22 September 2021
© Author(s) 2021. CC BY 4.0 License.


Deutsch, C., Sarmiento, J. L., Sigman, D. M., Gruber, N., and Dunne, J. P.: Spatial coupling of nitrogen inputs and losses in the ocean, Nature, 445, 163–167, doi:10.1038/nature05392, 2007.

Dunstan, P.K., Foster, S.D., King, E., Risbey, J., O'Kane, T. J., Monselesan, D., Hobday, A. J., Hartog J. R. and Thompson, P. A.: Global patterns of change and variation in sea surface temperature and chlorophyll a, Scientific Reports, 8, 14624. doi:10.1038/s41598-018-33057-y, 2018.

Eppley, R.W. and Peterson, B.J.: Particulate organic matter flux and planktonic new production in the deep ocean, Nature, 282, 677–680. doi:10.1038/282677a0, 1979.

Falkowski, P.G. and Kolber, Z.: Variations in chlorophyll fluorescence yields in phytoplankton in the world oceans, Functional Plant Biology, 22, 341–355. doi:10.1071/PP9950341, 1995.

Fennel, K. and Boss, E.: Subsurface maxima of phytoplankton and chlorophyll: Steady-state solutions from a simple model, Limnology and Oceanography, 48, 1521–1534. doi:10.4319/lo.2003.48.4.1521, 2003.

Frouin, R., Franz, B. and Werdell, P.: The SeaWiFS PAR product, Algorithm updates for the fourth SeaWIFS data reprocessing, 22, 46–50, 2003.

Fujiki, T., Inoue, R., Honda, M. C., Wakita, M., Mino, Y., Sukigara, C., and Abe, O.: Time-series observations of photosynthetic oxygen production in the subtropical western North Pacific by an underwater profiling buoy system, Limnology and Oceanography, 65, 1072–1084. doi:10.1002/lno.11372, 2020.

Furuya, K.: Subsurface chlorophyll maximum in the tropical and subtropical western Pacific Ocean: Vertical profiles of phytoplankton biomass and its relationship with chlorophyll a and particulate organic carbon, Marine Biology, 107, 529–539. doi:10.1007/BF01313438, 1990.

Garcia, H. E., Weathers, K., Paver, C. R., Smolyar, I., Boyer, T. P., Locarnini, R. A., Zweng, M. M., Mishonov, A. V., Baranova, O. K., Seidov, D., and Reagan, J. R.: World Ocean Atlas 2018, Volume 3: Dissolved Oxygen, Apparent Oxygen Utilization, and Oxygen Saturation, A. Mishonov Technical Ed.; NOAA Atlas NESDIS 83, 38pp, 2018.

Garcia, H. E., Weathers, K., Paver, C. R., Smolyar, I., Boyer, T. P., Locarnini, R. A., Zweng, M. M., Mishonov, A. V., Baranova, O. K., Seidov, D., and Reagan, J. R.: World Ocean Atlas 2018, Volume 4: Dissolved Inorganic Nutrients (phosphate, nitrate and nitrate+nitrite, silicate), A. Mishonov Technical Ed.; NOAA Atlas NESDIS 84, 35pp. 2018.

Goldman, J.C.: Spatial and temporal discontinuities of biological processes in pelagic surface waters, In: Rothschild B.J. (eds) Toward a theory on biological-physical interactions in the world ocean. NATO ASI Series (Series C: Mathematical and Physical Sciences), 239. Springer, Dordrecht. doi:10.1007/978-94-009-3023-0_15, 1988.

Gomi, Y., Taniguchi, A., and Fukuchi, M.: Temporal and spatial variation of the phytoplankton assemblage in the eastern Indian sector of the Southern Ocean in summer 2001/2002, Polar Biology, 30, 817–827. doi:10.1007/s00300-006-0242-2, 2007.

Itoh, S., Yasuda, I., Saito, H., Tsuda, A., and Komatsu, K.: Mixed layer depth and chlorophyll a: Profiling float observations in the Kuroshio-Oyashio Extension region, Journal of Marine Systems, 151, 1–14. doi:10.1016/j.jmarsys.2015.06.004, 2015

https://doi.org/10.5194/os-2021-88
Preprint. Discussion started: 22 September 2021
© Author(s) 2021. CC BY 4.0 License.


Jochum, M., Yeager, S., Lindsay, K., Moore, K., and R. Murtugudde, R.: Quantification of the Feedback between Phytoplankton and ENSO in the Community Climate System Model, Journal of Climate, 23, 2916–2925, doi:10.1175/2010JCLI3254.1, 2010.

Kang, X., Zhang, R. H., Gao, C., and Zhu, J.: An improved ENSO simulation by representing chlorophyll-induced climate feedback in the NCAR Community Earth System Model, Scientific Reports, 7, 17123. doi.org:10.1038/s41598-017-17390-2, 2017.

Karl, D. M., Christian, J. R., Dore, J. E., Hebel, D. V., Letelier, R. M., Tupas, L. M., and Winn, C. D.: Seasonal and interannual variability in primary production and particle flux at Station ALOHA, Deep Sea Research Part II, 43, 539–568. doi:10.1016/0967-0645(96)00002-1, 1996.

Karl, D., Letelier, R., Tupas, L., Dore, J., Christian, J., and Hebel, D.: The role of nitrogen fixation in biogeochemical cycling in the subtropical North Pacific Ocean, Nature, 388, 533–538. doi:10.1038/41474, 1997.

Landry, M. R., Barber, R. T., Bidigare, R. R., Chai, F., Coale, K. H., Dam, H. G., Lewis, M. R., Lindley, S. T., McCarthy, J. J., Roman, M. R., Stoecker, D. K., Verity, P. G., and White, J. R.: Iron and grazing constraints on primary production in the central equatorial Pacific: An EqPac synthesis, Limnology and Oceanography, 42, 405–418. doi:10.4319/lo.1997.42.3.0405, 1997.

Lee, K. W., Yeh, S. W., Kug, J. S., and Park, J. Y.: Ocean chlorophyll response to two types of El Niño events in an ocean-biogeochemical coupled model, Journal of Geophysical Research: Oceans, 119, 933–952. doi:10.1002/2013JC009050, 2014.

Letelier, R. M., Karl, D. M., Abbott, M. R. and Bidigare, R.R.: Light driven seasonal patterns of chlorophyll and nitrate in the lower euphotic zone of the North Pacific Subtropical Gyre, Limnology and Oceanography, 49, 508–519. doi:10.4319/lo.2004.49.2.0508, 2004.

Lewis, M. R., Hebert, D., Harrison, W. G., Platt, T. and Oakey, N. S.: Vertical nitrate fluxes in the oligotrophic ocean, Science, 234, 870–873. doi:10.1126/science.234.4778.870, 1986.

Lewis, M. R., Carr, M. -E., Feldman, G. C., Esaias, W., and McClain. C. R.: Influence of penetrating solar radiation on the heat budget of the equatorial Pacific Ocean, Nature, 347, 543–545. doi:10.1038/347543a0, 1990.

Lin, P., Chai, F., Xue, H., and Xiu, P.: Modulation of decadal oscillation on surface chlorophyll in the Kuroshio Extension, Journal of Geophysical Research: Oceans, 119, 187–199. doi:10.1002/2013JC009359, 2014.

Mann, K. H. and Lazier, J. R.: Dynamics of marine ecosystems: Biological-physical interactions in the ocean, 2nd ed., Blackwell Sci., Mal-den, Mass. doi:10.1017/S0025315400072003, 1996.

Maritorena, S., d'Andon, O.F., Mangin, A., and Siegel, D.: Merged satellite ocean color data products using a bio-optical model: Characteristics, benefits and issues, Remote Sensing of Environment, 114, 1791–1804. doi:10.1016/j.rse.2010.04.002, 2010.

Martin, J., and Fitzwater, S.: Iron deficiency limits phytoplankton growth in the north-east Pacific subarctic. Nature, 331, 341–343. doi:10.1038/331341a0, 1988.

https://doi.org/10.5194/os-2021-88
Preprint. Discussion started: 22 September 2021
© Author(s) 2021. CC BY 4.0 License.


Martin, J., Knauer, G., Karl, D., and Broenkow, W.: VERTEX: Carbon cycling in the northeast Pacific, Deep Sea Research, 34, 267–285. doi:10.1016/0198-0149(87)90086-0, 1987.

Martin, J., Gordon, R. and Fitzwater, S.: Iron in Antarctic waters, Nature, 345, 156–158. doi:10.1038/345156a0, 1990.

Masuda, Y., Yamanaka, Y., Smith, S.L., Hirata, T., Nakano, H., Oka, A., and Sumata, H.: Photoacclimation by phytoplankton determines the distribution of global subsurface chlorophyll maxima in the ocean, Communications Earth and Environment, B, 128. doi:10.1038/s43247-021-00201-y, 2021.

Matsumoto K. and Furuya, K.: Variations in phytoplankton dynamics and primary production associated with ENSO cycle in the western and central equatorial Pacific during 1994-2003, Journal of Geophysical Research, 116, C12042. doi:10.1029/2010JC006845, 2011.

Mignot, A., Claustre, H., Uitz, J., Poteau, A., D'Ortenzio, F., and Xing, X.: Understanding the seasonal dynamics of phytoplankton biomass and the deep chlorophyll maximum in oligotrophic environments: A Bio-Argo float investigation, Global Biogeochemical Cycles, 28, doi:10.1002/2013GB004781, 2014.

Moeller, H. V., Laufkötter, C., Sweeney, E. M., and Johnson, M. D.: Light-dependent grazing can drive formation and deepening of deep chlorophyll maxima, Nature Communications, 10, 1978, doi:10.1038/s41467-019-09591-2, 2019.

Moore, T. S., Matear, R. J., Marra, J. and Clementson, L.: Phytoplankton variability off the Western Australian Coast: Mesoscale eddies and their role in cross-shelf exchange, Deep Sea Research Part II, 54, 943–960. doi:10.1016/j.dsr2.2007.02.006, 2007.

Nishioka, J. and Obata, H.: Dissolved iron distribution in the western and central subarctic Pacific: HNLC water formation and biogeochemical processes, Limnology and Oceanography, 62, 2004–2022, 2017.

Olsen, A., Lange, N., Key, R. M., Tanhua, T., Álvarez, M., Becker, S., Bittig, H. C., Carter, B. R., Cotrim da Cunha, L., Feely, R. A., van Heuven, S., Hoppema, M., Ishii, M., Jeansson, E., Jones, S. D., Jutterström, S., Karlsen, M. K., Kozyr, A., Lauvset, S. K., Lo Monaco, C., Murata, A., Pérez, F. F., Pfeil, B., Schirnick, C., Steinfeldt, R., Suzuki, T., Telszewski, M., Tilbrook, B., Velo, A., and Wanninkhof, R.: GLODAPv2.2019—An update of GLODAPv2. Earth System Science Data, 11, 1437–1461. doi:10.5194/essd-11-1437-2019, 2019.

Pedlosky J.: The dynamics of the oceanic subtropical gyres, Science, 248, 316–322. doi:10.1126/science.248.4953.316, 1990.

Park, J. Y., J. P. Dunne, and C. A. Stock: Ocean chlorophyll as a precursor of ENSO: An earth system modeling study. Geophysical Research Letters, 45, 1939–1947, doi:10.1002/2017GL076077, 2018.

Rayner, N. A. A., Parker, D. E., Horton, E. B., Folland, C. K., Alexander, L. V., Rowell, D. P., Kent, E. C., and Kaplan, A.: Global analyses of sea surface temperature, sea ice, and night marine air temperature since the late nineteenth century. Journal of Geophysical Research, 108, 4407, doi:10.1029/ 2002JD002670, 2003.

Riser, S.C. and Johnson, K.S.: Net production of oxygen in the subtropical ocean, Nature, 451, 323–325. doi:10.1038/nature06441, 2008.

Saijo, Y., Iizuka, S., and Asaoka, O.: Chlorophyll maxima in Kuroshio and adjacent area, Marine Biology, 4, 190–196. doi:10.1007/BF00393892, 1969.

© Author(s) 2021. CC BY 4.0 License.


Sasaoka, K., Chiba, S., and Saino, T.: Climatic forcing and phytoplankton phenology over the subarctic North Pacific from 1998 to 2006, as observed from ocean color data. Geophysical Research Letters, 38, L15609. doi:10.1029/2011GL048299, 2011.

Séférian, R., Berthet, S., Yool, A. et al.: Tracking Improvement in Simulated Marine Biogeochemistry Between CMIP5 and CMIP6, Current Climate Change Reports, 6, 95–119, doi:10.1007/s40641-020-00160-0, 2020.

Siegel, D.A., Ohlmann, J.C., Washburn, L., Bidigare, R.R., Nosse, C.T., Fields, E., and Zhou, Y.: Solar radiation, phytoplankton pigments and the radiant heating of the equatorial Pacific warm pool, Journal of Geophysical Research, 100, 4885–4891. doi:10.1029/94JC03128, 1995.

Sverdrup, H. U.: On conditions for the vernal blooming of phytoplankton, ICES Journal of Marine Science, 18, 287–295. doi:10.1093/icesjms/18.3.287, 1953.

Trenberth, K. E.: The definition of El Niño, Bulletin of the American Meteorological Society, 78, 2771–2778. doi:10.1175/1520-0477(1997)078<2771:TDOENO>2.0.CO;2, 1997.

Uitz, J., Claustre, H., Morel, A., and Hooker, S. B.: Vertical distribution of phytoplankton communities in open ocean: An assessment based on surface chlorophyll, Journal of Geophysical Research, 111, 1–23. http://doi.org/10.1029/2005jc003207, 2006.

Yasunaka, S., Nojiri, Y., Nakaoka, S., Ono, T., Mukai, H., and Usui, N.: Monthly maps of sea surface dissolved inorganic carbon in the 695 North Pacific: Basin-wide distribution and seasonal variation, Journal of Geophysical Research: Oceans, 118, 3843–3850. http://doi.org/10.1002/jgrc.20279, 2013.

Yasunaka, S., Mitsudera, H., Whitney, F., and Nakaoka, S.: Nutrient and dissolved inorganic carbon variability in the North Pacific. Journal of Oceanography, 77, 3–16. doi:10.1007/s10872-020-00561-7, 2021.

Yoder, J. A.: Effect of temperature on light-limited growth and chemical composition of Skeletonema costatum (Bacillariophyceae), Journal of Phycology, 15, 362–370. doi:10.1111/j.1529-8817.1979.tb00706.x, 1979.

https://doi.org/10.5194/os-2021-88
Preprint. Discussion started: 22 September 2021
© Author(s) 2021. CC BY 4.0 License.

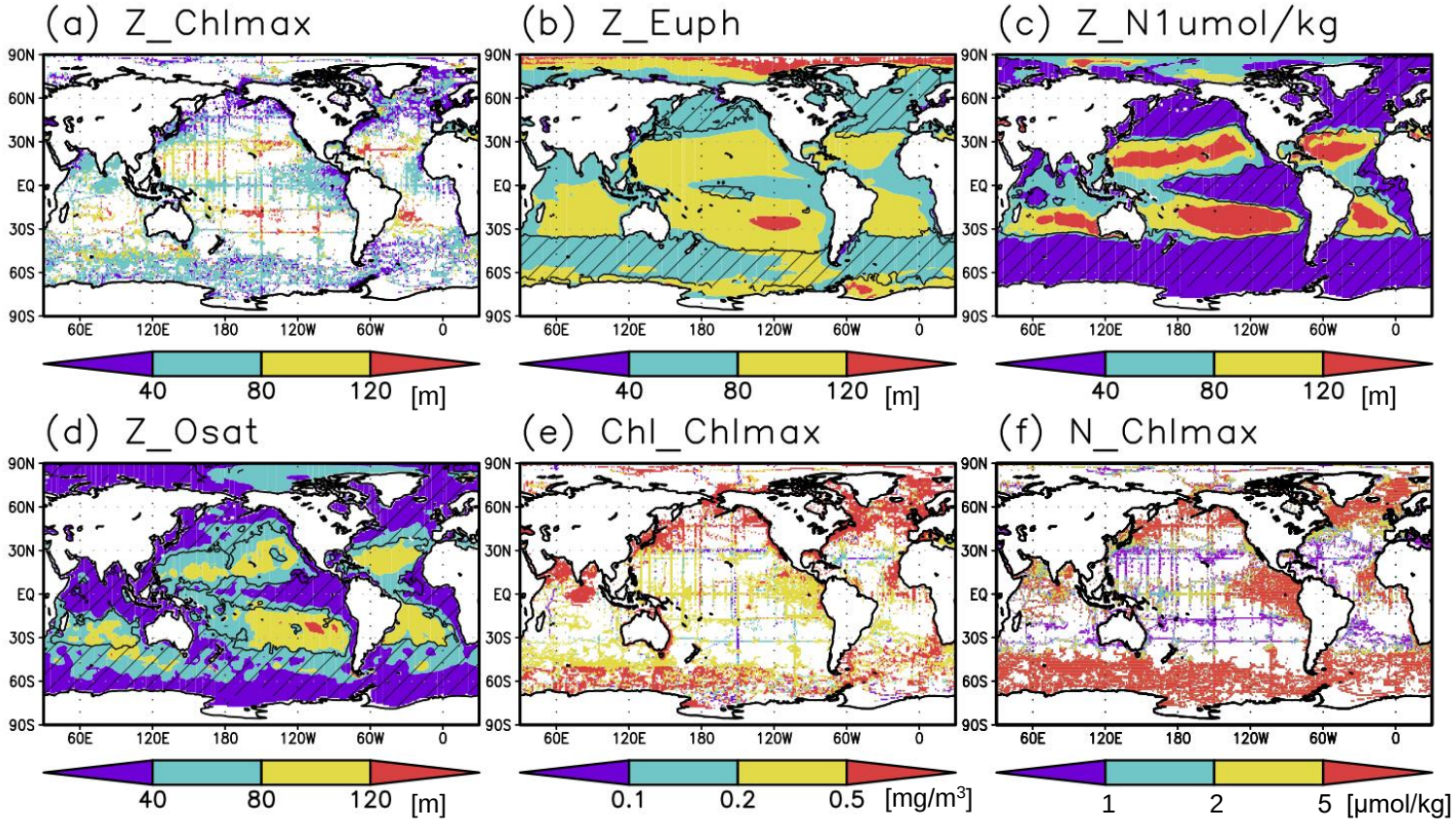

Figure 1: (a–d) Depths of the chlorophyll *a* (Chl-*a*) maximum, euphotic layer, nitrate depleted layer (<1 µmol/kg of nitrate), and oxygen oversaturated layer, respectively. (e and f) Chl-*a* and nitrate concentrations at the Chl-*a* maximum. The hatched areas show that the mixed layer is deeper than the euphotic layer in panel (b), nitrate deplete layer in panel (c), and oxygen saturation layer in panel (d).

https://doi.org/10.5194/os-2021-88
Preprint. Discussion started: 22 September 2021
© Author(s) 2021. CC BY 4.0 License.

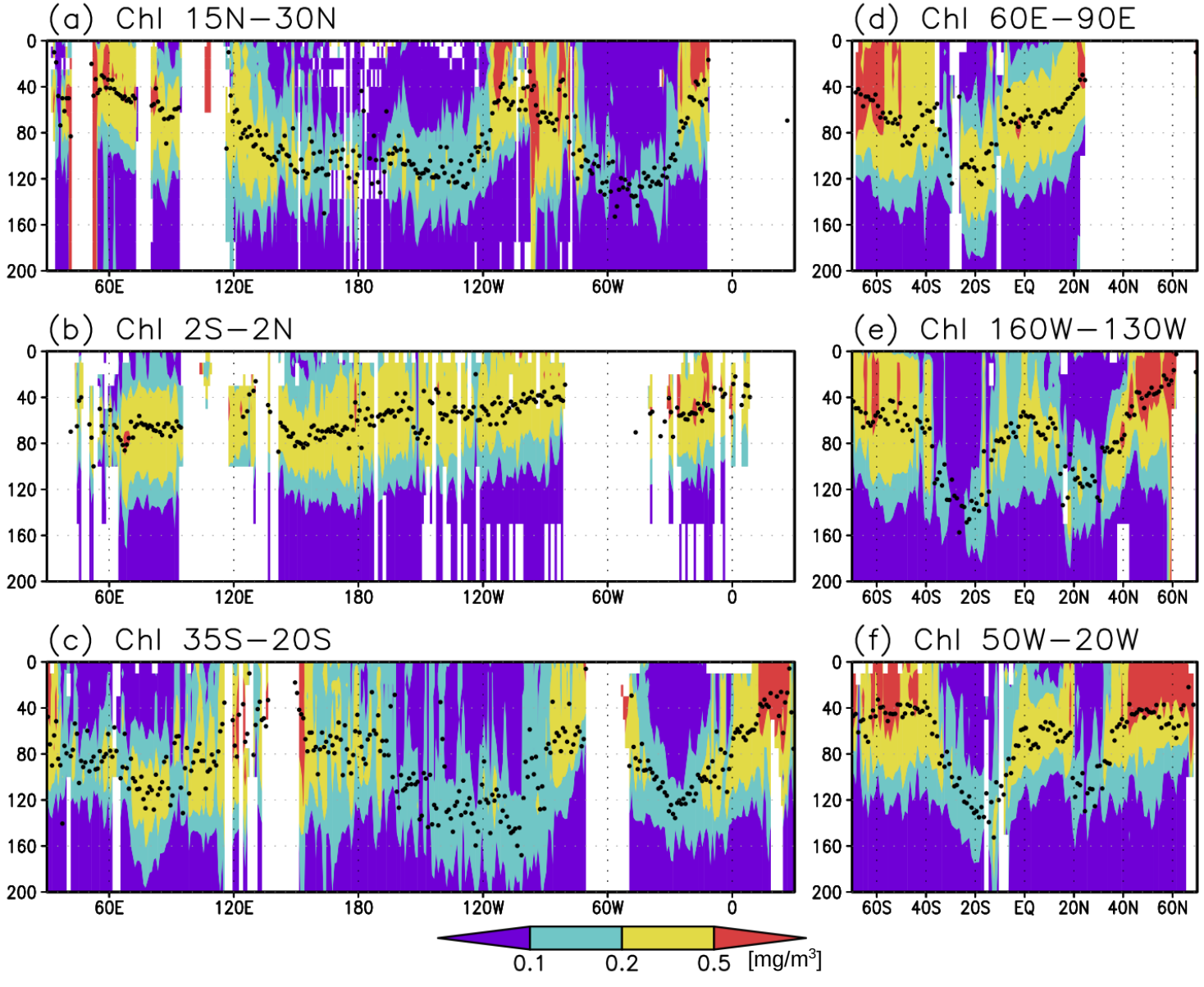

Figure 2. Cross-sections of chlorophyll *a* (Chl-*a*) concentrations at (a) 15–30°N (northern subtropics), (b) 2°S to 2°N (tropics), (c) 35–20°S (southern subtropics), (d) 60–90°E (the Indian Ocean), (e) 160–130°W (the Pacific Ocean), and (f) 50–20°W (the Atlantic Ocean). The black dot shows the depth of the Chl-a maximum.

https://doi.org/10.5194/os-2021-88
Preprint. Discussion started: 22 September 2021
© Author(s) 2021. CC BY 4.0 License.

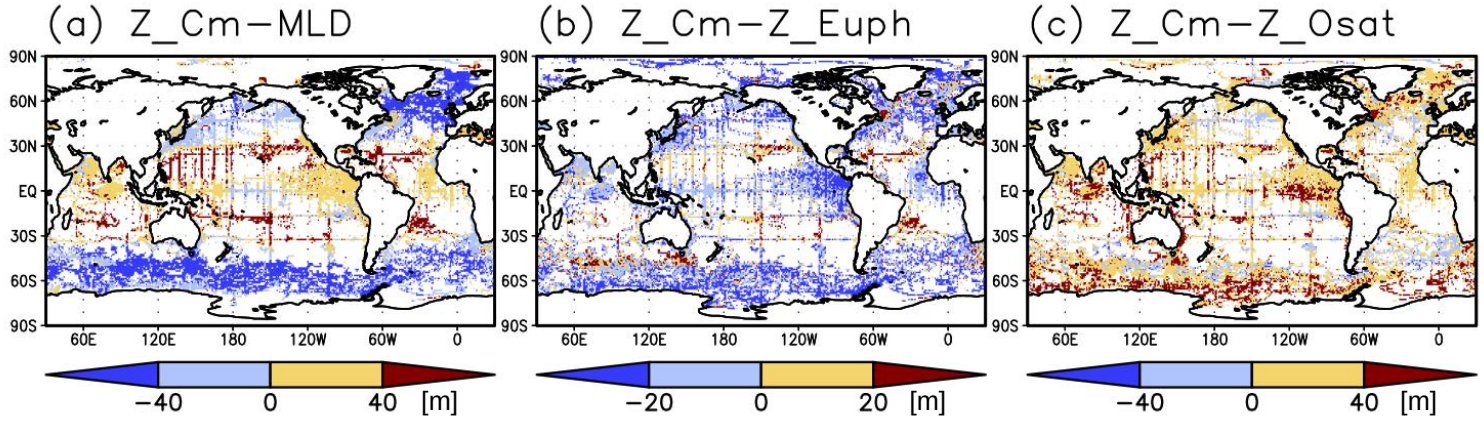

415

Figure 3. Depth difference between the chlorophyll *a* (Chl-*a*) maximum and (a) mixed layer, (b) euphotic layer, and (c) oxygen oversaturated layer.

https://doi.org/10.5194/os-2021-88
Preprint. Discussion started: 22 September 2021
© Author(s) 2021. CC BY 4.0 License.

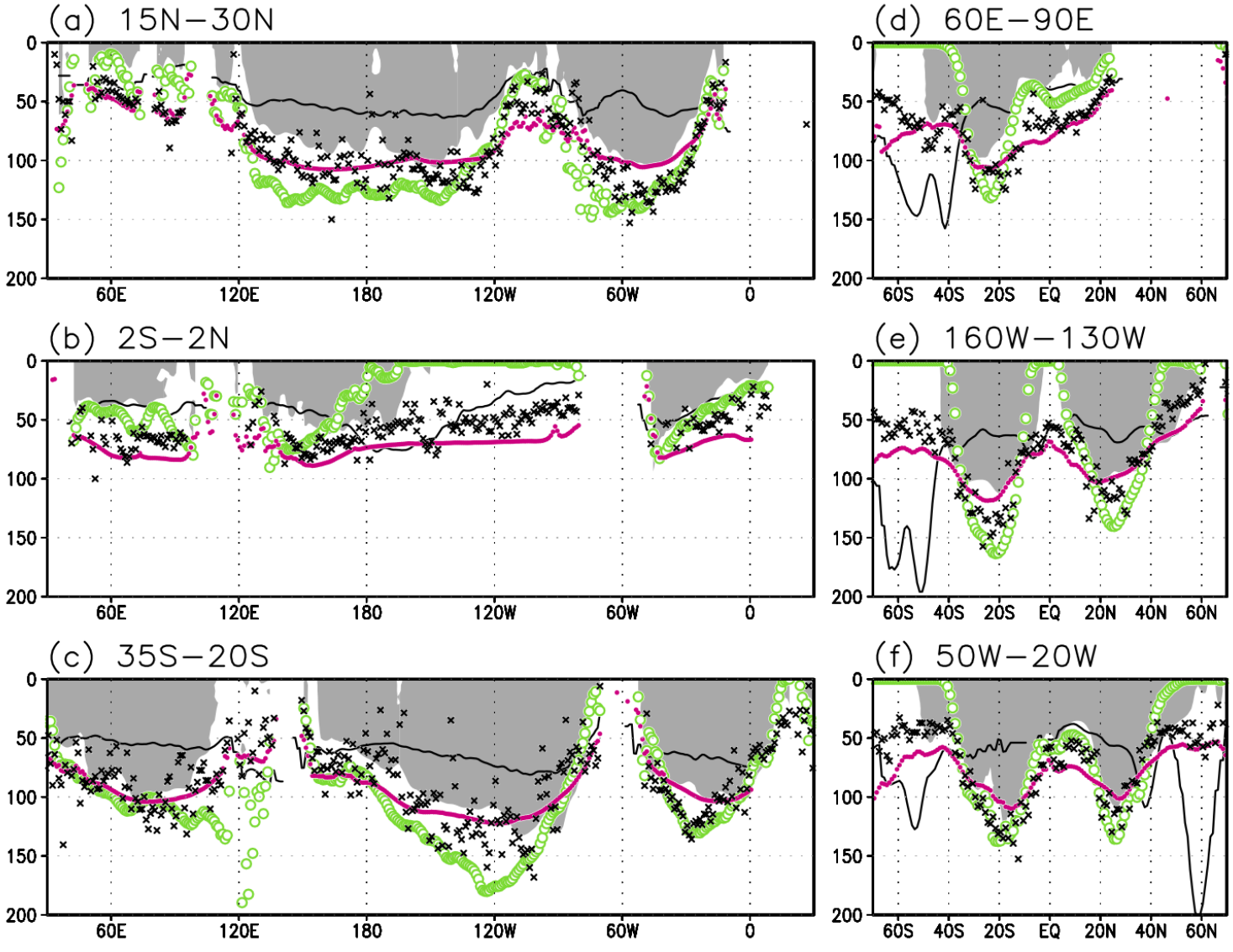

420

Figure 4. Depths of the chlorophyll *a* (Chl-*a*) maximum (black cross), euphotic layer (magenta dot), nitrate depleted layer (<1 µmol/kg of nitrate; green open circle), mixed layer (black line), and oxygen oversaturated layer (gray hatch) at (a) 15–30°N (northern subtropics), (b) 2°S to2°N (tropics), (c) 35–20°S (southern subtropics), (d) 60–90°E (Indian Ocean), (e) 160–130°W (Pacific Ocean), and (d) 50–20°W (Atlantic Ocean).

425

https://doi.org/10.5194/os-2021-88
Preprint. Discussion started: 22 September 2021
© Author(s) 2021. CC BY 4.0 License.

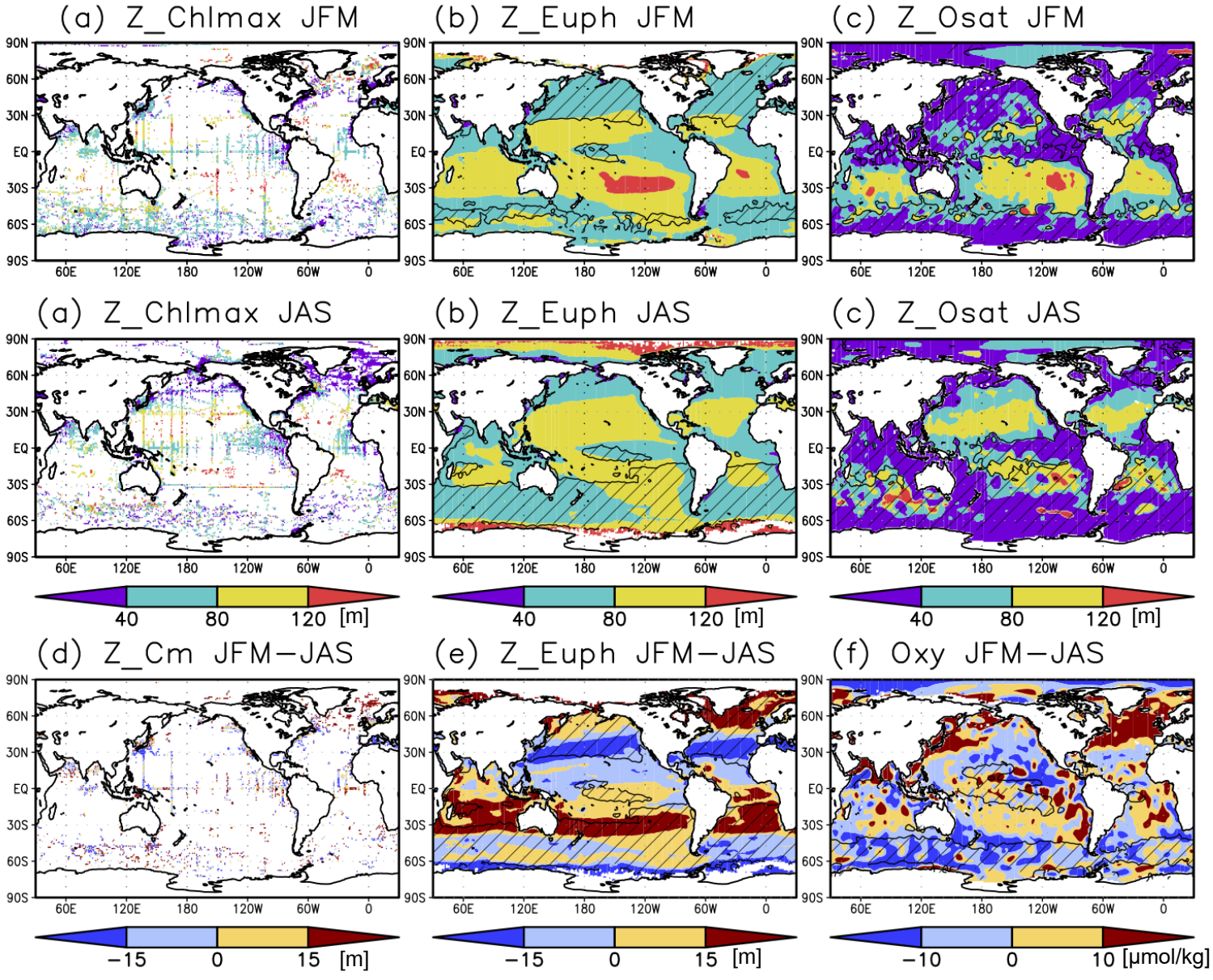

Figure 5. (a–c) Depths of the chlorophyll *a* (Chl-*a*) maximum, euphotic layer, and oxygen oversaturated layer in January–March (JFM) (top) and July–September (JAS) (middle), respectively. (d–f) Differences between Chl-a maximum depth, euphotic layer depth, and dissolved oxygen concentration at 50–150 m in JFM and those in JAS. The hatched areas show that the mixed layer is deeper than the euphotic layer in panel (b), oxygen saturation layer in panel (c), euphotic layer in winter in panel (e), and 50 m in summer in panel (f).

https://doi.org/10.5194/os-2021-88
Preprint. Discussion started: 22 September 2021
© Author(s) 2021. CC BY 4.0 License.

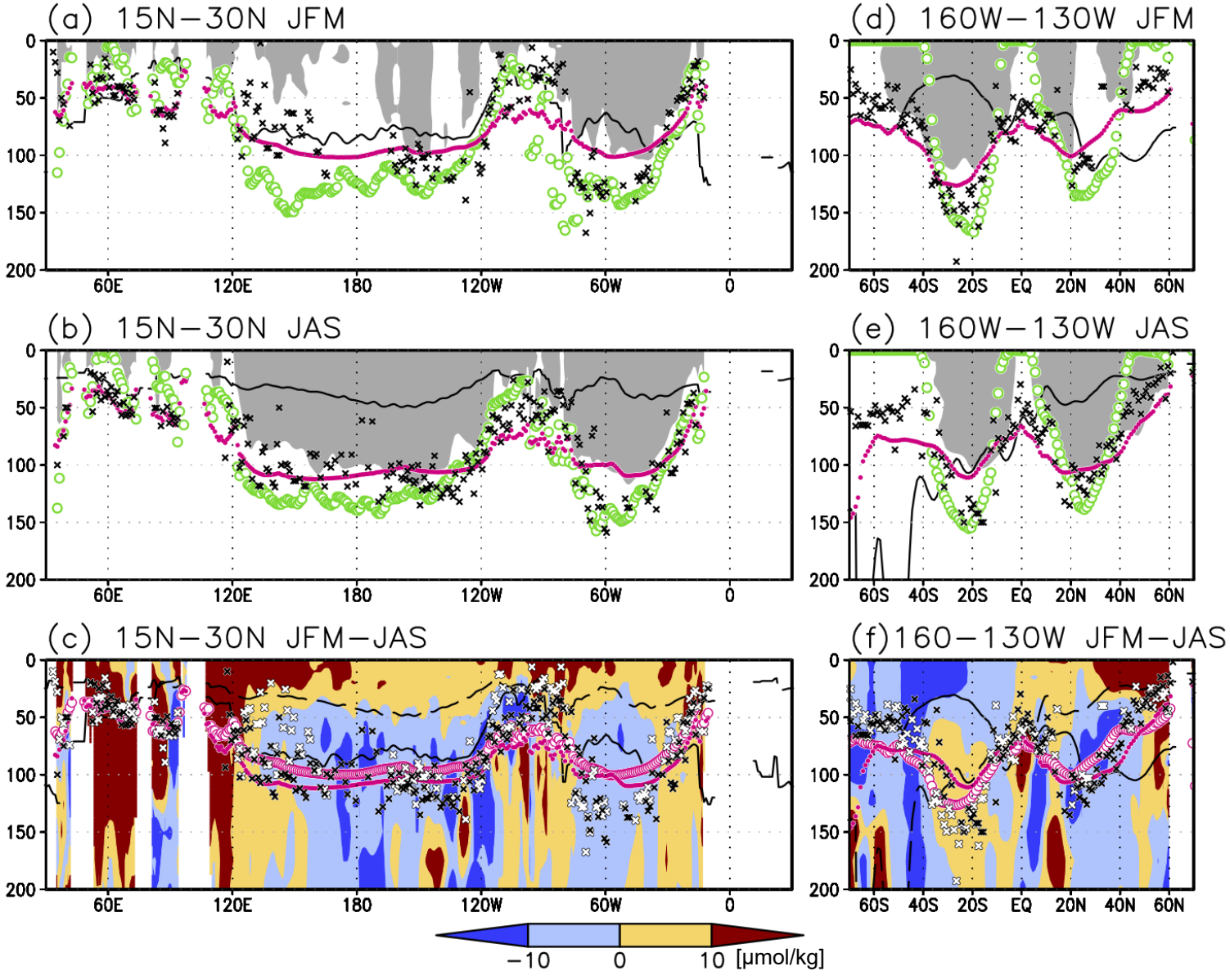

Figure 6. (a, b) Depths of the chlorophyll *a* (Chl-*a*) maximum (black cross), euphotic layer (magenta dot), nitrate depleted layer (<1 μmol/kg of nitrate; green open circle), mixed layer (black line), and oxygen oversaturated layer (gray hatch) at 15–30°N (northern subtropics) in (a) January–March (JFM) and (b) July–September (JAS). (c) Difference between dissolved oxygen concentration in JFM and that in JAS (shade), and depths of the Chl-*a* maximum, euphotic layer, and mixed layer in JFM and JAS (white and black crosses, magenta opened and closed dots, and solid and dashed black line, respectively) at 15–30°N. (d–f) Same as (a–c), but at 160–130°W (Pacific Ocean).

https://doi.org/10.5194/os-2021-88
Preprint. Discussion started: 22 September 2021
© Author(s) 2021. CC BY 4.0 License.

Ocean Science
Discussions
Open Access
EGU

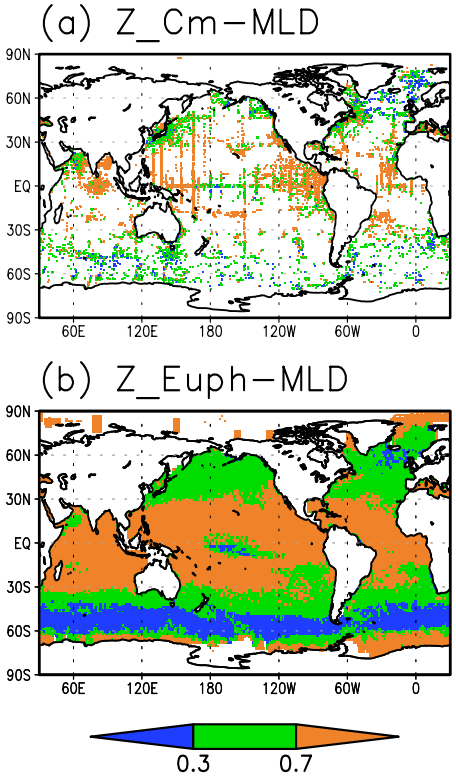

Figure 7. (a, b) Ratio of months when the chlorophyll *a* (Chl-*a*) maximum (a) and the euphotic layer (b) were deeper than the mixed layer. Data in grids with only one datum are omitted

https://doi.org/10.5194/os-2021-88
Preprint. Discussion started: 22 September 2021
© Author(s) 2021. CC BY 4.0 License.

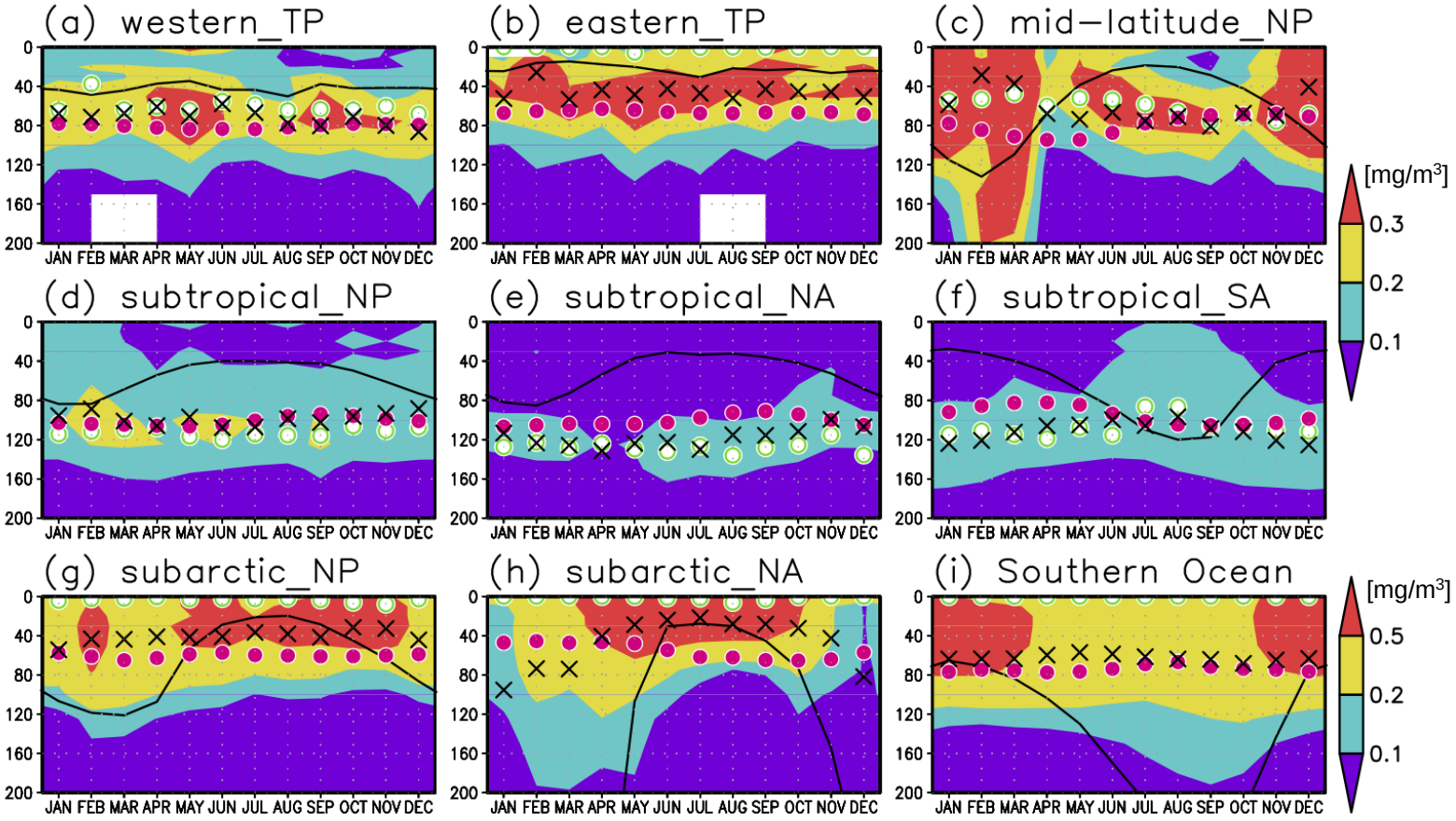

Figure 8. Seasonal evolution of chlorophyll *a* (Chl-*a*) concentrations with the Chl-a maximum (black cross), euphotic layer (magenta dot), 1 µmol/kg of nitrate (green open circle), and mixed layer (black solid line) at (a) 2°S to 2°N, 120–170°E (western tropical Pacific), (b) 2°S to 2°N, 120–90°W (eastern tropical Pacific), (c) 30–40°N, 150-130°W (midlatitude North Pacific), (d) 10–30°N, 120°E to 120°W (subtropical North Pacific), (e) 15–30°N, 70–30°W (subtropical North Atlantic), (f) 30–10°S, 50–0°W (subtropical South Atlantic), (g) 40–55°N, 160°E to 155°W (subarctic North Pacific), (h) 50–70°N, 30–0°E (subarctic North Atlantic), and (i) 60–45°S (Southern Ocean).

https://doi.org/10.5194/os-2021-88
Preprint. Discussion started: 22 September 2021
© Author(s) 2021. CC BY 4.0 License.

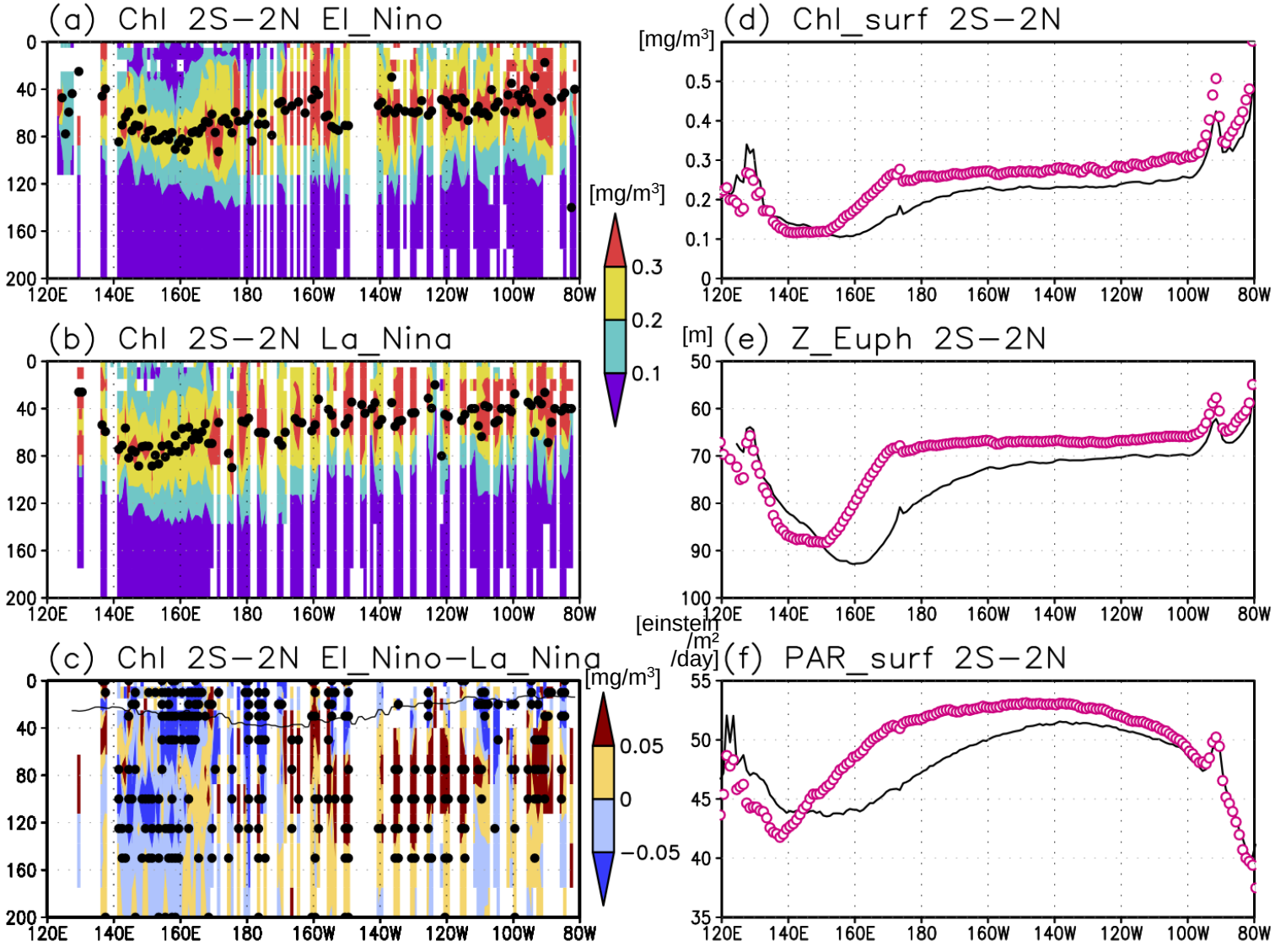

Figure 9. (a–c) Cross-sections of the chlorophyll *a* (Chl-*a*) concentrations in the equatorial Pacific (2°S to 2°N) during El Niño and La Niña, and the difference between them. The black dot denotes the depth of the Chl-*a* maximum in panels (a) and (b), and the significant difference in Chl-*a* concentration at 5% in panel (c). The black line denotes mixed layer depths for all years in panel (c). (d) Satellite-derived surface Chl-*a* concentration, (e) euphotic layer depth, and (f) surface photosynthetically active radiation along the equatorial Pacific during El Niño (black solid line) and La Niña (magenta open circle).